5-2013

Localized Meshless Methods With Radial Basis Functions For Eigenvalue Problems

Amy M. Kern

The University of Southern Mississippi

LOCALIZED MESHLESS METHODS WITH RADIAL BASIS FUNCTIONS FOR EIGENVALUE PROBLEMS

by

Amy Kern

A Thesis
Submitted to the Honors College
of the University of Southern Mississippi
in Fulfillment
of the Requirement for the Degree of
Bachelor of Science
in the Department of Mathematics

April 2013

.

Approved:

Dr. Huiqing Zhu
Advisor, Assistant Professor of Mathematics

Dr. Sungwook Lee
Interim Chair, Department of Mathematics

Dr. David R. Davies
Dean, Honors College

ACKNOWLEDGMENTS

This is to thank all of those who have assisted me in this effort. First of all, I would like to thank my advisor, Dr. Zhu, for all of the time and effort he has put into working with me on my thesis. I have learned an incredible amount from him about not only mathematics, but also about the research process. I am so very grateful to him for all that he has taught me over the past year, and for his patience and encouragement throughout this process.

Secondly, I would like to thank my thesis defense committee from the Department of Mathematics- Dr. Lyle, Dr. Perry, and Dr. Tian. I greatly appreciate all of the comments, suggestions, and questions that I have received.

In addition, I would like to thank Dr. Stephan Howden of the University of Southern Mississippi's Department of Marine Science for providing the original inspiration for my thesis, assistance with the irregular domain application, and all of the many fruitful discussions we have had. I have learned so much about applied mathematics in marine science from working with him.

I would also like to thank my family-my mom, dad, and four sisters- for all of their love and support throughout this process and throughout my entire academic career. They have taught me so many life lessons that have molded me into the person I am today. I could not have gotten here without all that they have done for me.

Finally, I would like to thank my friends- Molly Gunnels, Carmen Wingerter, Michelle Pontiff, Lauren Dutton, and Matthew Franszczak- who provided me with countless fun times and great memories to keep me going through tough times. Their friendship has truly been a blessing.

ABSTRACT

LOCALIZED MESHLESS METHODS WITH RADIAL BASIS FUNCTIONS FOR EIGENVALUE PROBLEMS

by Amy Kern

April 2013

Two localized meshless methods with radial basis functions are considered for solving eigenvalue problems on two different domains, i.e., a L-shaped domain and an irregular domain. The irregular domain used in this study comes from an application of the eigenvalue problem as it plays a role in the reconstruction of velocity vector fields. This study finds that both localized Kansa's method and the Localized Method of Approximate Particular Solutions provide a good numerical approximation to the solution of the eigenvalue problem. Through numerical experiments, a good value for the shape parameter can be determined for each domain for each method which will minimize the relative error and maximum relative error in the eigenvalues of the numeric approximation. The relative error and maximum relative error were calculated for each domain using different grid sizes. In addition, the convergence rates for both methods were determined for both domains, and appear to be quite similar.

TABLE OF CONTENTS

LIST OF ILLUSTRATIONS

Figure

LIST OF TABLES

Table

Chapter 1

BACKGROUND

1.1 Introduction

Partial differential equations (PDE) have applications in a vast number of areas including fluid dynamics, mechanics, computational physics and applied mathematics. Since so many fields use partial differential equations, being able to find accurate solutions to partial differential equations is very important in many areas. However, finding an analytical solution is not possible for all PDEs. In place of finding an analytical solution, researchers have developed many different methods for numerical approximations of PDE solutions.

This thesis will focus on the numerical solution of eigenvalue problems. In many textbooks, it is referred to as the *Helmholtz equation*. The Helmholtz equation often arises in the study of physical problems involving PDEs in both space and time, e.g., electromagnetic wave propagation and acoustics. The Helmholtz equation, which represents the time-independent form of the original equation, results from applying the technique of separation of variables to reduce the complexity of the analysis. For example, in [9], the circular drumhead problem is originally posed as a two-dimensional wave equation on the unit circle with Dirichlet boundary conditions. However, in searching for the solution, separation of variables is performed on the wave equation to transform it into the Helmholtz boundary value problem

$$\Delta U + \lambda^2 U = 0 \qquad \text{in unit disk,}$$

$$U(1,\theta) = 0 \qquad 0 \leq \theta < 2\pi.$$

Although the Helmholtz equation is not typically the direct problem being solved, it still has many applications. In fact, the author later explained that by factoring the time component

out of the heat equation, the solution to the Helmholtz equation is needed once more to resolve that problem [9]. Since it appears frequently in application problems of many forms, finding an accurate solution to the Helmholtz equation is very important.

We will use localized meshless methods with radial basis functions to approximate the solution of eigenvalue problems on two different domains, i.e., a L-shaped domain and an irregular domain. The irregular domain will be tied to the application of using partial differential equations to try to reconstruct a velocity vector field (cf. Section 1.3). This application is one example of how methods, such as the ones used in this study, can be used in real world problems. However, before delving into the specifics, one should have a basic understanding of all the associated concepts. The first question one might ask is: What is the general eigenvalue problem? According to [2], the eigenvalue problem can be expressed as

$$\mathcal{A}\psi = \lambda\psi \tag{1.1.1}$$

where $\mathcal{A}$ is a linear operator whose domain and range is a Hilbert space, ψ is a vector or a function in the space, and λ is a constant. In this case, the operator $\mathcal{A}$ is known, and the unknowns are ψ, the eigenvectors or eigenfunctions, and λ, the eigenvalues. Eigenfunctions and their corresponding eigenvalues compose the solution to the eigenvalue problem.

In (1.1.1), $\mathcal{A}$ is defined to be a linear operator. For the purposes of our study, $\mathcal{A}$ will be the Laplacian operator $\Delta = \frac{\partial^2}{\partial x^2} + \frac{\partial^2}{\partial y^2}$. This study will seek to calculate the eigenvalues λ and the eigenfunctions ψ that provide the solution to

$$\begin{aligned} \Delta u + \lambda u &= 0 \qquad \text{in } \Omega, \\ u &= 0 \qquad \text{on } \partial\Omega, \end{aligned} \tag{1.1.2}$$

where Ω is a bounded region in $\mathbb{R}^2$ and $\partial\Omega$ represents its boundary.

As [8] notes, one important characteristic to note about the eigenvalues from (1.1.2) is

Theorem 1.1.1. 1. Each eigenvalue of Problem (1.1.2) is real;

2. Furthermore, if we repeat each eigenvalue according to its (finite) multiplicity, we have a list of eigenvalues:

$$\{\lambda_k\}_{k=1}^{\infty},$$

where

$$0 < \lambda_1 \leq \lambda_2 \leq \lambda_3 \leq \cdots,$$

and

$$\lambda_k \to \infty, \quad \text{as} \quad k \to \infty.$$

As a result of this theorem, the solution to the eigenvalue problem includes a list of real-valued eigenvalues which can be listed, with repeated values, in ascending order, and all values will be greater than zero.

According to [21], eigenvalue problems, like the one in this study, occur in acoustics and, as such, can be defined on complicated domains including ones involving corners. The more complicated the domain is, the more challenging finding a solution can be. When an approximation method, like finite difference method, finite element method, or meshless methods that use radial basis functions, is implemented, the eigenvalue problem is expressed in terms of matrices, which we usually call “discrete problems". A discrete version of Problem (1.1.2) can be rewritten as

$$A\boldsymbol{v} = \tilde{\lambda}\boldsymbol{v}, \tag{1.1.3}$$

or, in other words,

$$(\tilde{\lambda}I - A)\boldsymbol{v} = 0 \tag{1.1.4}$$

where A is a matrix of finite dimensions; I denotes the identity matrix of the same size. Equation (1.1.4) will have nontrivial solutions if

$$\det(\tilde{\lambda}I - A)\boldsymbol{v} = 0. \tag{1.1.5}$$

According to [1], “This is called the characteristic equation of A; the scalars satisfying this equation are the eigenvalues of A. When expanded, the determinant is always a polynomial of $\tilde{\lambda}$. $\cdots$ It follows from the Fundamental Theorem of Algebra that the characteristic equation has at most n distinct solutions so A has at most n distinct eigenvalues."

The discrete problem (1.1.3) derived from different numerical methods is an approximation to Problem (1.1.2). The eigenvalues of Problem (1.1.3) is denoted by $\tilde{\lambda}$. The number of eigenvalues $\tilde{\lambda}$ depends on the size of matrix A. A good numerical method will produce numerical eigenvalues that are accurate approximations to some of eigenvalues of Problem (1.1.2) (cf. [3, 26]).

1.2 A Short Literature Review

Over the years, many different methods have be used to find the eigenvectors and eigenvalues for the eigenvalue problem. These numerical procedures include traditional and advanced numerical methods, such as finite element method (FEM) [3, 24], finite difference method [16], spectral method [26], moment method [14], multipole expansion technique [25], and meshless methods [6, 10], etc. FEM solves the weak form of PDEs, while finite difference method and meshless methods solve the strong form of PDEs. The first step of FEM is mesh generation. In this step, a reasonable mesh is created , consisting of triangles or other polygons, that are called “elements". Mesh nodes, edges, and local information associated to each element will be stored in different arrays. This step is simplified in meshless methods to the generation of collocation points. Also, when discretizing PDEs, meshless methods don’t involve numerical integration,which makes them computationally faster than FEM. In [3], the finite element method is used on the L-shaped domain to find solutions to the eigenvalue problem with Neumann boundary condition. They display their calculated eigenvalues in comparison to the exact eigenvalues and find that the approximation increases in accuracy with more elements in the unstructured triangular mesh. However, in order to increase the number of elements, the mesh must be refined. Keeping up with the maintainence of

the mesh is one of the main disadvantages of using a method like Finite Element Method. Nevertheless, Boffi concludes that the convergence of the method is quadratic [3] when piecewise linear polynomials are employed.

In regards to meshless methods, one of the oldest meshless methods appears to be the smooth particle hydrodynamics (SPH) method developed in 1977. SPH was initially developed for astrophysical problems [18]. Later, Gingold and Monaghan developed further foundation for the method through the use of kernel approximations [20]. Since the late 1970s and early 1980s, many variations and advancements have been made in the field of meshless methods leading up to the two meshless methods this study will focus on. In 1990 Kansa [12] designed the radial basis function (RBF) collocation method for solving elliptical, hyperbolic and parabolic PDEs. Later on this approach (Kansa's method) was extended to various PDEs, including nonlinear PDEs. In 2003, Platte and Driscoll [22] applied the global RBF-collocation method to eigenvalue problems with elliptic operators. One of the domains used in [22] is an L-shaped domain. As this is one of the domains that this study will utilize, particular attention will be given to their results on this domain. In their study, Platte and Driscoll studied a radial basis function method with the multiquadric RBF and enforced both Dirichlet and Neumann boundary conditions. The multiquadric RBF takes two parameters- a distance between two points and a positive constant value called the shape parameter, which will be further defined in the following chapters. Nevertheless, Driscoll and Platte presented results using a "shape parameter" of 0.6 because, even though accuracy improves with larger value "shape parameters," the matrix becomes ill-conditioned. In addition, as mentioned in their algorithm, they add additional functions to their radial basis function approximation in order to account for corner singularities because the regular radial basis function approximation did not converge and clustering nodes at the corners did not help. In order to add these additional functions, certain characteristics of the eigenfunction had to be exploited. When the maximum relative error for the first twelve eigenvalues was calculated using the global Kansa's method and no added functions for corner singularities,

the maximum relative error was consistently greater than a magnitude of 10^{-2}. When additional functions were added for corner singularities, the maximum error was able to drop to a magnitude of 10^{-3} in some cases [22]. In their conclusion, Platte and Driscoll write, "For the L-shaped domain and the rhombus, the inclusion of singular terms was found to be essential for good convergence rates."

MAPS that was designed by Chen et. al in [5] stems from the Method of Particular Solutions. This method have similar properties to integrated RBFs-collocation methods. When global radial basis function methods are employed, no mesh creation or refinement is necessary. However the global matrices formed by the radial basis function approximations are plagued by ill-conditioning, especially when a large number of collocation points are necessary. In this study, collocation points are data locations arbitrarily placed within the domain where function values are to be approximated through the use of radial basis collocation methods. Typically, irregular domains require a large number of collocation points. Moreover, for irregular domain, such as a general polygon, extra terms of corner singularities to enrich the basis functions are not available. It seems that if certain RBFs are used, the most important technique to obtain an accurate numerical approximation is to increase the number of collocation points. In this situation, localized methods will be more desirable because, by using a localized radial basis functions method, the matrices will be sparse instead of dense. In this way, the issues present with other methods can be avoided by using localized domains. For more details about localized meshless methods using RBFs, we refer the reader to [5, 27, 28].

1.3 An Application: To Reconstruct Velocity Vector Field on The Northern Gulf of Mexico

In the field of physical oceanography, high frequency radars are used to gather information about the surface currents of a body of water. However, the data sets gathered from the high frequency radars are plagued by changes in range over time, data drop outs, and

downtime resulting in data gaps at various locations at random times. Having an incomplete data set is very inconvenient when a researcher is trying to run a time series analysis that requires a continuous data set. In such cases, the data set must be interpolated in time and/or interpolated or extrapolated in space in order to fill in the gaps. During the BP oil spill in 2010, researchers studying the Gulf of Mexico faced this issue because, at the time of the spill, only one of three high frequency radars were operating [11]. These researchers were being turned to by the local, state, and federal governments to use their data sets to choose which model would best predict the oil's dispersion. While researchers were able to get the other two high frequency radars running within a week's time, the gaps in the data set created increased uncertainty in the choosing of a model [11]. While the data that was available was helpful to the oil spill management, a complete data set would have been even more helpful.

Since this is a common problem for many research projects, researchers have put a lot of time and effort into developing many different methods to try to estimate the missing data in the vector fields. In 2004, Lekien et. al proposed a process which they refer to as "open-boundary modal analysis" (OMA) and which uses the Lipphardt et. al method as a foundation on which to build their method [15, 17]. One way that OMA differs from the other methods used by Lipphardt et. al and Chu et. al is that it attempts to account for flow across the open boundaries of the data collection area without requiring an "a priori knowledge of the normal velocity at the open boundary" [15, 7, 17]. In addition, OMA involves the calculation of interior and boundary modes based on the geometry of the geographical domain. OMA is the first of the three methods to have boundary modes as opposed to simply a boundary condition for the modes. Once these modes are calculated for a certain domain, they can be reused for nowcasting at a later time on the same domain [15]. In regards to the term "nowcasting", Lekien explains that it is a "reference to the much more common forecasting option. Nowcasting does not involve the extrapolation of the velocity into the future. It uses the available data to determine the velocity everywhere in space at

the same time the data were collected" [15]. The only part of OMA that involves the actual CODAR data and the nowcast velocity field is the calculation of the projection coefficients. Finding the coefficients necessitates the solving of an $N \times N$ system of equations where N is number of boundary, incompressible, and irrotational modes used in the nowcast [15]. In this manner, OMA significantly decreases the amount of computation that was required by the Chu et. al and Lipphardt et. al methods in [7, 17].

Taking a CODAR data set from Monterey Bay, Lekien et. al proceeded to test their open boundary modal analysis. Along with the data set, they used PLTMG, a software package for solving elliptic partial differential equations. The eigenfunctions found through PTLMG are intended to be used on a domain that uses an “unstructured triangular grid" [15].The use of the unstructured triangular grid is another improvement on the method proposed by Lipphardt et. al which employed the “use of a staircase approximation of the coastline" [15].

Part of using the OMA method to create nowcasts of the velocity field requires the solving of an eigenvalue problem with Dirichlet boundary conditions and an eigenvalue problem with Neumann boundary conditions [15]. OMA uses the finite element method as its tool for solving the eigenvalue problem. However, in the proposed study, two newer meshless method will be used to solve the eigenvalue problem with Dirichlet boundary conditions. These methods have the benefit of not needing to approximate the domain boundaries in order to get an accurate solution in a timely manner. While OMA is not implemented in this study, the study will test how the two meshless methods would perform on an irregular domain like those that might use OMA. Once we get the eigenvalues and eigenfunctions on this irregular domain, the velocity field could be reconstructed.

1.4 Proposed Study and Hypothesis

The proposed study will solve the eigenvalue boundary value problem with Dirichlet boundary conditions, as given in (1.1.2), for two different domains.

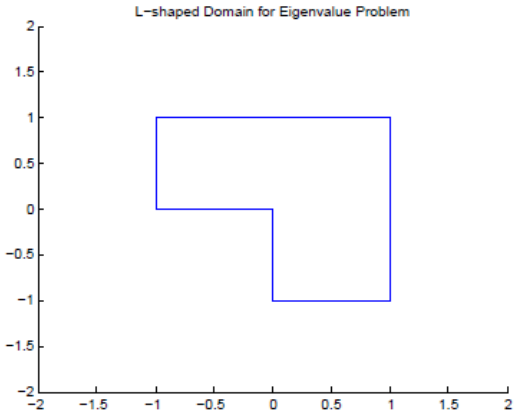

Figure 1.1: L-shape domain.

The first domain is an enclosed L-shape where

$$\Omega_1 = [-1,1]^2 \setminus [-1,0]^2.$$

Figure 1.1 sketched the graph of this domain.

The second domain is a part of the application of reconstructing a velocity vector field by solving the eigenvalue problem with boundary conditions. To construct this domain, a time step of surface current data was found for which there was a maximum number of velocity vectors measured in the northern Gulf of Mexico. The latitudes and longitudes where the data was collected were extracted, and the boundary locations were identified to form an irregular shape that closely mimics the shape of the area of data collection (see Figure 1.2).

This study will use two different methods, i.e., localized Kansa's method and Localized Method of Approximate Particular Solution (LMAPS), to find a numerical solution to the partial differential equation defined in (1.1.2). Both of the methods in this study are based on a global form of the same method, i.e., Kansa's method and Method of Approximate Particular Solution (MAPS) which are elaborated on in Section 2.2. The variation of Kansa's

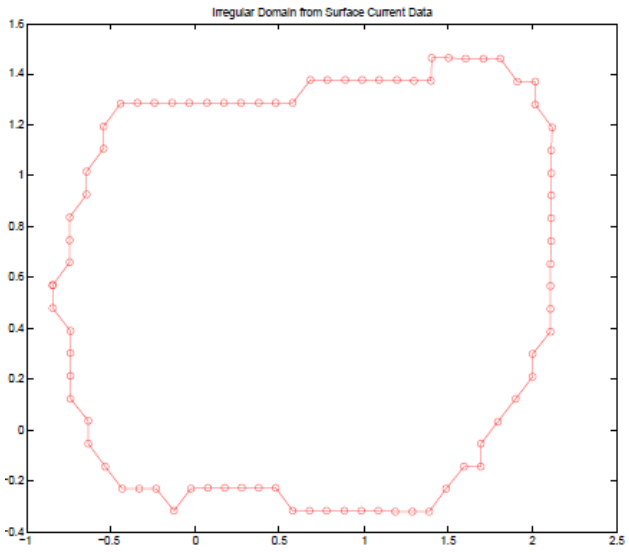

Figure 1.2: Irregular Domain

method which will be utilized in this study is localized Kansa's Method which is introduced in Section 2.3. LMAPS is a more recent method which will be briefly explained in Section 2.3. Localized Method of Approximate Particular Solution was chosen for this study because this method is expected to yield results with a higher accuracy than in [22] and to avoid the necessity of adding singular terms in order to reach this degree of accuracy. In addition, since it is a localized method, the matrices formed during the method will not suffer from ill-conditioning because they will be sparse matrices. Finally, this method will not require a mesh but will still take the domain into account and yield results of a certain degree of accuracy. The localized Kansa's method is being used to provide a comparison for the results of the LMAPS.

Using these two methods, this study proposes to calculate the first ten eigenvalues and their corresponding numerical eigenfunctions. The first ten eigenvalues for both methods

will be displayed in Section 3.1 for the L-shaped domain and Section 3.2 for the irregular domain. In addition to calculating the solution to the partial differential equation in (1.1.2), an analysis will be performed to determine how the "shape parameter" affects the relative error and the maximum relative error in the eigenvalues. The results of this analysis are displayed in Section 4.1. This study is also interested in comparing the stability of the error in regards to different "shape parameters" across methods to see if one method is significantly more favorable than the other one. Also, the convergence rates for the two methods will be determined and discussed in Section 4.2.

The goals on this study are as follows:

- Goal 1: To determine if localized Kansa's method and LMAPS are good methods for solving the eigenvalue problem on the L-shaped domain and the irregular domain. In the past, a number of methods, including FEM and radial basis collocation method, have been used on the L-shaped domain and produced fairly accurate results. So far, no known study has tested localized Kansa's method or LMAPS on either of the two domains presented in this study. Therefore, this study seeks to provide some data for these methods on the given domains.

- Goal 2: To figure out the value(s) that the "shape parameter" of the multiquadric radial basis function that will minimize error and provide stability to the numeric solution for both the irregular and L-shaped domain. A lot of work is currently being performed to find a method for how to pick a good "shape parameter." As this seems to still be a question for research, this study will test a variety of "shape parameters" and analyze the results.

- Goal 3: To decide what size local domain will produce the most accurate results for the irregular domain.

This study hopes to provide some insight into these three main topics upon its conclusion.

Chapter 2

Methodology

A number of different methods are available for finding numerical solutions to a partial differential equation like the eigenvalue problem (1.1.2) that is the focus of this study. As was mentioned in [15], one method that can be used involves the formation of an unstructured triangular mesh on the domain of the PDE. The method Lekien is referring to is more formally known as the Finite Element Method where the triangles of the mesh are considered to be the elements. While the Finite Element Method has been used for decades to solve problems in science and engineering, the generation and maintenance of the mesh is a substantial drawback to using this method and other similar mesh-based methods. In the more recent years, researchers have made drastic progress in the creation of meshless methods for numerical solutions. In [27], Yao explains “Meshless methods, in contrast, use the geometry of the domain directly to avoid many of the difficulties which characterize meshed and grided methods." Some of these meshless methods depend on a group of functions referred to as radial basis functions which are particularly useful in numerical approximations and interpolations. Yao points out that "The main advantages of RBF-based methods for solving partial differential equations lie in their simplicity, their applicability to various PDEs, and their effectiveness in dealing with high-dimensional problems with complicated geometries" [27]. In particular, this study will utilize two RBF-based methods called localized Kansa’s method and Localized Method of Approximate Particular Solutions (LMAPS) to solve the eigenvalue problem with Dirichlet boundary conditions on each of the two previously defined domains.

2.1 Radial basis functions (RBFs)

Radial basis functions (RBFs) comprise the foundation for the numerical methods employed by this study, and, therefore, it is essential to have a firm grasp of what the radial basis functions are. The history of the concept of radial basis functions dates back to near 1985 and 1986 when they were discussed by both Powell [23] and Micchelli [19]. One of the first uses of radial basis functions was in a study by Broomhead and Lowe in 1988 for their work on adaptive networks [4]. Using more recent mathematical terminology, Yao provides a definition of a RBF in her dissertation.

Definition 2.1.1. Let $\mathbb{R}^d$ be d-dimensional Euclidean space. Let $\boldsymbol{p} \in \mathbb{R}^d$, and let $\phi : \mathbb{R}^d \to \mathbb{R}$ be an invariant function whose value at any point $\boldsymbol{x} \in \mathbb{R}^d$ depends only on the distance from the fixed point $\boldsymbol{p}$, and can be written

$$\phi(\|\boldsymbol{x} - \boldsymbol{p}\|)$$

Then the function ϕ is a RBF where $\boldsymbol{p}$ is the center of the RBF ϕ [27].

While this notation may be appropriate for a formal definition, in many papers, the RBF is denoted as $\phi(r)$ where $r = \|\boldsymbol{x} - \boldsymbol{p}\|$. For the remainder of this study, the radial basis function will be indicated as $\phi(r)$. The Euclidean norm will be utilized in this study, and is what is intended by $\|\cdot\|$. Table 2.1 gives a number of examples of RBFs. Here constant

Table 2.1: Examples of Radial Basis Functions

RBF Names	Formula
linear	r
cubic	r^3
Gaussian	$\exp(-r^2)$
Multiquadrics	$\sqrt{r^2 + c^2}$
Inverse Multiquadrics	$1/\sqrt{r^2 + c^2}$
Thin-plate spline	$r^2 ln(r)$

$c > 0$ is called the *shape parameter* of RBFs.

The way to implement using a RBF is to identify a finite set of distinct points $\{\boldsymbol{p}_j\}_{j=1}^{N}$ in $\mathbb{R}^n$. In the given definition of a RBF, each one of the points in this set is a center of a RBF. Collectively, these centers can be used to give a RBF approximation of a function u:

$$\tilde{u}(\boldsymbol{x}) := \sum_{j=1}^{N} \alpha_j \phi(\|\boldsymbol{x} - \boldsymbol{p}_j\|), \tag{2.1.1}$$

where $\boldsymbol{x} \in \mathbb{R}^n$.

Let us review about how to find the RBF interpolation $\tilde{u}$. In [22], Platte explains that "If $u(\boldsymbol{x}_i)$, $i = 1, 2, \cdots, N$, were known, finding $\boldsymbol{\alpha}$ would require the solution of an $N \times N$ linear system

$$A\boldsymbol{\alpha} = \boldsymbol{U},$$

where

$$A = [\phi(\|\boldsymbol{x}_i - \boldsymbol{p}_j\|)]_{N\times N},$$
$$\boldsymbol{\alpha} = [\alpha_1, \alpha_2, ..., \alpha_N]^T,$$
$$\boldsymbol{U} = [u(\boldsymbol{x}_1), u(\boldsymbol{x}_2), ..., u(\boldsymbol{x}_N)]^T.$$

Matrix A is called the RBF interpolation matrix and, for some RBFs, is positive definite."

As this study utilizes the multiquadric RBF, particular interest is given to its behaviors. In [27],Yao states a few more useful properties of the multiquadrics radial basis functions (MQ-RBFs): “This is a class of monotonically increasing functions of distance r. It has been prove that the MQ is conditionally positive definite and of order one, which implies that the matrix for the interpolation problem is invertible." We will only use the MQ-RBF in the analysis and numerical experiments.

One noteworthy characteristic of RBFs is that the error calculated from using RBFs to approximate a smooth function approaches zero rather quickly. As a result of these high convergence rates, using RBFs typically equates to needing fewer collocation points to get an accurate approximation [27]. These characteristics further promote the use of radial basis function methods, like LMAPS and Kansa’s method.

2.2 Method of Approximated Particular Solutions (MAPS) and Kansa's method

We will sketch the idea of MAPS and Kansa's method in this section. These two different methods were designed for PDEs, such as the Possion equation $\Delta u = f$. In Kansa's method, we use RBF approximation from Equation (2.1.1) to approximate u so that f can be approximated by $\Delta\tilde{u}$. In MAPS, the right hand side f utilizes the RBF approximation in Equation (2.1.1), which is the same as $\tilde{u}$ in Kansa's method. Therefore, the RBF approximation of $\tilde{u}$ in MAPS is the combination $\sum \alpha_j \Phi_j$, since Φ_j is a particular solution of ϕ_j.

It has been observed that MAPS is more stable and accurate for solving Possion equation than Kansa's method. Thus, it will be interesting to see if these two methods give comparable numerical results for eigenvalue problems. First, we will briefly explain the method of finding the RBF approximation $\tilde{u}$ to the exact solution of Problem (1.1.2) regardless of the type of RBFs, which will be specified later.

Suppose that radial basis functions Φ and ϕ satisfy

$$\Delta\Phi = \frac{1}{r}\frac{d}{dr}\left(r\frac{d}{dr}\Phi\right) = \phi.$$

Hence, if we use radial basis function Φ in the RBF interpolation (2.1.1), it follows that

$$\begin{aligned} \tilde{u}(\boldsymbol{x}) &= \sum_{j=1}^{N} \alpha_j \Phi(\|\boldsymbol{x} - \boldsymbol{p}_j\|), \\ \Delta\tilde{u}(\boldsymbol{x}) &= \sum_{j=1}^{N} \alpha_j \phi(\|\boldsymbol{x} - \boldsymbol{p}_j\|). \end{aligned} \tag{2.2.1}$$

Place the set of points $\{\boldsymbol{p}_j\}_1^N = \{\boldsymbol{x}_j\}_1^N$, which is the set of collocation points both in the domain and on the boundary. The interior points will be denoted as $\{\boldsymbol{x}_j\}_1^{N_i}$, and the collocation points on the boundary will be denoted as $\{\boldsymbol{x}_j\}_{N_i+1}^{N_i+N_b}$ such that $N = N_i + N_b$. The entire set of collocation points will be used to approximate the solution $u(\boldsymbol{x})$ to the PDE.

Substituting u in (1.1.2) with $\tilde{u}$ and confining the equation to the set of collocation points,

we have

$$\begin{aligned} -\sum_{j=1}^{N} \alpha_j \phi(\|\boldsymbol{x}_i - \boldsymbol{x}_j\|) &= \lambda \sum_{j=1}^{N} \alpha_j \Phi(\|\boldsymbol{x}_i - \boldsymbol{x}_j\|) \qquad \forall\, i = 1, \cdots, N_i, \\ \sum_{j=1}^{N} \alpha_j \Phi(\|\boldsymbol{x}_i - \boldsymbol{x}_j\|) &= 0 \qquad\qquad\qquad\qquad\quad \forall\, i = N_i + 1, \cdots, N. \end{aligned} \tag{2.2.2}$$

The above equations define a linear system with variable $\boldsymbol{\alpha}$. For simplicity, we can write it into a matrix form:

$$A\boldsymbol{\alpha} = \lambda B\boldsymbol{\alpha}, \tag{2.2.3}$$

where

$$A = \begin{pmatrix} L^I \\ P \end{pmatrix}, \qquad B = \begin{pmatrix} A^I \\ 0_{N_b \times N} \end{pmatrix}.$$

Here L^I, A^I, P are matrices defined as follows:

$$L^I = [\phi(\|\boldsymbol{x}_i - \boldsymbol{x}_j\|)]_{N_I \times N}, \qquad A^I = [\Phi(\|\boldsymbol{x}_i - \boldsymbol{x}_j\|)]_{N_I \times N}, \qquad P = [\Phi(\|\boldsymbol{x}_i - \boldsymbol{x}_j\|)]_{N_b \times N}$$

Solving (2.2.2) we obtain N values of λ. Multiple eigenvalues are possible. The eigenvalues of (2.2.2) are the N smallest eigenvalues of Problem (1.1.2).

Now we are going to point out the radial basis functions used in Kansa's method and MAPS.

In Kansa's method, we let Φ be the multiquadrics RBF, and solve (2.2.3) with $\Delta\Phi = \phi$ so that ϕ takes the following value

$$\Phi = \sqrt{r^2 + c^2}, \qquad \phi = \frac{2}{\sqrt{r^2 + c^2}} - \frac{r^2}{(r^2 + c^2)^{3/2}}. \tag{2.2.4}$$

But in MAPS method, we let ϕ be the multiquadrics RBF. We solve (2.2.3) by using the

following values for ϕ and Φ:

$$\Phi = \frac{4c^2+r^2}{9}\sqrt{r^2+c^2} - \frac{c^3}{3}ln(c+\sqrt{r^2+c^2}), \qquad \phi = \sqrt{r^2+c^2}. \tag{2.2.5}$$

2.3 LMAPS and localized Kansa's method

In this study, radial basis functions will be utilized in a method called the Localized Method of Approximate Particular Solutions (LMAPS) which was first introduced in [27, 28] and is a more recent approach to MAPS. In MAPS, the basis functions for an approximate solution to the original partial differential equation are found by using radial basis functions $\phi(r)$ to find a solution to, in the case of this study, $\Delta\Phi(r) = \phi(r)$ [27]. However, it should be noted that the method is not restricted to the use of Δ as the operator. As demonstrated in the previous section, the downfall of MAPS is the fact that the approximations are found by using all of the collocations points which results in dense matrices that are ill-conditioned and sensitive to the choice of shape parameter [27]. By using LMAPS, this study hopes to avoid these added difficulties. LMAPS uses the same basis functions as are found in MAPS for the approximation, but, instead of using all the collocation points, a local domain is found for each collocation point. The local domain consists of the n nearest neighbors to that point. By only using the local domain to approximate a solution at each point, the dense matrix in MAPS becomes a sparse matrix in LMAPS which reduces the ill-conditioning. Also, in [27], Yao states, "Another important advantage of local RBF approaches is that the MQ or IMQ shape parameter affects the numerical results only slightly." For these reasons, this study has chosen to use the LMAPS method. However, before proceeding further, it may be helpful to look at the mathematics involved in LMAPS. Similarly, instead of Kansa's method, we will also use the localized Kansa's method and compare it with LMAPS. To begin, the general method will be introduced followed by the appropriate functions to use for each method given that, as in this study, the multiquadric RBF is to be used.

We use the set of collocation points $\{\boldsymbol{x}_j\}_1^N$ defined in Section 2.2. The interior points will

be denoted as $\{\boldsymbol{x}\}_1^{N_i}$, and the collocation points on the boundary will be denoted as $\{\boldsymbol{x}\}_{N_i+1}^{N_i+N_b}$ such that $N = N_i + N_b$. For each $\boldsymbol{x}_s$ in the set of collocation points, a local domain must be found of the nearest n neighbors. Here we will adopt Yao's notation for demonstrating the local domain of a collocation point $\boldsymbol{x}_s$ as $\boldsymbol{x}_k^{[s]}$ for $k = 1, 2, \cdots, n$ [27]. In this notation, all the $\boldsymbol{x}_k^{[s]}$ with the same s value denote being a part of the same local domain Ω_s for $\boldsymbol{x}_s$, and k denotes which of n-nearest neighbors it is. It is important to note that the local domains for different collocation points can and, in most cases, will overlap with each other.

Within the local domain Ω_s of an interior point x_s ($s = 1, \cdots, N_i$), the function values of u can be approximated by the local RBF interpolation:

$$u(\boldsymbol{x}) \approx \tilde{u}(\boldsymbol{x}) = \sum_{k=1}^{n} \alpha_k^{[s]} \Phi(\|\boldsymbol{x} - \boldsymbol{x}_k^{[s]}\|). \tag{2.3.1}$$

Setting $\boldsymbol{x} \in \{\boldsymbol{x}_k^{[s]}\}_1^n$ yields a system of equations

$$\begin{bmatrix} \tilde{u}(\boldsymbol{x}_1^{[s]}) \\ \tilde{u}(\boldsymbol{x}_2^{[s]}) \\ \vdots \\ \tilde{u}(\boldsymbol{x}_n^{[s]}) \end{bmatrix} = \begin{bmatrix} \Phi(\|\boldsymbol{x}_1^{[s]} - \boldsymbol{x}_1^{[s]}\|) & \Phi(\|\boldsymbol{x}_1^{[s]} - \boldsymbol{x}_2^{[s]}\|) & \ldots & \Phi(\|\boldsymbol{x}_1^{[s]} - \boldsymbol{x}_n^{[s]}\|) \\ \Phi(\|\boldsymbol{x}_2^{[s]} - \boldsymbol{x}_1^{[s]}\|) & \Phi(\|\boldsymbol{x}_2^{[s]} - \boldsymbol{x}_2^{[s]}\|) & \ldots & \Phi(\|\boldsymbol{x}_2^{[s]} - \boldsymbol{x}_n^{[s]}\|) \\ \vdots & \vdots & \ldots & \vdots \\ \Phi(\|\boldsymbol{x}_n^{[s]} - \boldsymbol{x}_1^{[s]}\|) & \Phi(\|\boldsymbol{x}_n^{[s]} - \boldsymbol{x}_2^{[s]}\|) & \ldots & \Phi(\|\boldsymbol{x}_n^{[s]} - \boldsymbol{x}_n^{[s]}\|) \end{bmatrix} \begin{bmatrix} \alpha_1^{[s]} \\ \alpha_2^{[s]} \\ \vdots \\ \alpha_n^{[s]} \end{bmatrix}.$$

For ease of referencing, the above equation can be rewritten as

$$\boldsymbol{U}^{[s]} = P_{nn} \boldsymbol{\alpha}^{[s]},$$

where

$$P_{nn} = \left[\Phi(\|\boldsymbol{x}_i^{[s]} - \boldsymbol{x}_j^{[s]}\|)\right], \quad \boldsymbol{\alpha}^{[s]} = \left(\alpha_1^{[s]}, \cdots, \alpha_n^{[s]}\right)^T, \quad \boldsymbol{U}^{[s]} = \left(\tilde{u}(\boldsymbol{x}_1^{[s]}), \cdots, \tilde{u}(\boldsymbol{x}_n^{[s]})\right)^T.$$

From here it's easy to see that

$$\boldsymbol{\alpha}^{[s]} = P_{nn}^{-1}\boldsymbol{U}^{[s]}. \tag{2.3.2}$$

Let

$$\boldsymbol{\Phi}^{s} = \left[\Phi(\|\boldsymbol{x}_s - \boldsymbol{x}_1^{[s]}\|), \Phi(\|\boldsymbol{x}_s - \boldsymbol{x}_2^{[s]}\|), \cdots, \Phi(\|\boldsymbol{x}_s - \boldsymbol{x}_n^{[s]}\|)\right],$$
$$\boldsymbol{\Psi}^{s} = \left[\phi(\|\boldsymbol{x}_s - \boldsymbol{x}_1^{[s]}\|), \phi(\|\boldsymbol{x}_s - \boldsymbol{x}_2^{[s]}\|), \cdots, \phi(\|\boldsymbol{x}_s - \boldsymbol{x}_n^{[s]}\|)\right].$$

Using (2.2.1) and (2.3.2) we obtain

$$\Delta\tilde{u}(\boldsymbol{x}_s) = \Delta\boldsymbol{\Phi}^{[s]}\boldsymbol{\alpha}^{[s]} = \boldsymbol{\Psi}^{[s]}P_{nn}^{-1}\boldsymbol{U}^{[s]} = \Theta^{[s]}\boldsymbol{U}^{[s]} = \Theta\boldsymbol{U}, \tag{2.3.3}$$

where

$$\Theta^{[s]} = \boldsymbol{\Psi}^{[s]}P_{nn}^{-1}, \qquad \boldsymbol{U} = (\tilde{u}(\boldsymbol{x}_1), \cdots, \tilde{u}(\boldsymbol{x}_{N_i}))^T,$$

and, to transition from the local domains to the global function values, $N-n$ zeroes are placed within vectors $\Theta^{[s]}$ (which becomes Θ) at locations where the function values are not included in the local domain.

Then the approximation problem using localized method directly follows (2.3.3) and the fact that the right-hand side is nothing but a single vector $\Theta\boldsymbol{U}$:

$$\Theta\boldsymbol{U} = \lambda\boldsymbol{U}. \tag{2.3.4}$$

The first m eigenvalues and corresponding numerical eigenfunctions of the above linear system can be solved by using MATLAB command $eigs(\Theta, m, 0)$.

Remark 2.3.1. In localized Kansa's Method, we let Φ be the multiquadrics RBF, and solve (2.3.3) with $\Delta\Phi = \phi$ so that ϕ takes the following value

$$\Phi = \sqrt{r^2 + c^2}, \qquad \phi = \frac{2}{\sqrt{r^2 + c^2}} - \frac{r^2}{(r^2 + c^2)^{3/2}}. \tag{2.3.5}$$

But in LMAPS method, we let ϕ be the multiquadrics RBF. We solve (2.3.3) by using

the following values for ϕ and Φ:

$$\Phi = \frac{4c^2 + r^2}{9}\sqrt{r^2 + c^2} - \frac{c^3}{3} ln(c + \sqrt{r^2 + c^2}), \qquad \phi = \sqrt{r^2 + c^2}. \tag{2.3.6}$$

Chapter 3

Numerical Experiments

The eigenvalue problem that is being numerically solved in this study was introduced at the beginning of Chapter 1 in (1.1.2). Then, in Chapter 1 Section 4, the domains used in this study were defined to be an L-shaped domain as well as an irregular shaped domain derived from the domain of surface current data in the northern Gulf of Mexico. To elaborate on the previously defined basis of this study, the population of the collocation points must be discussed as this is a crucial part of any method that utilizes radial basis functions. The methods for defining the collocation points will be described in the following sections.

3.1 Example 1: L-shape Domain

By using the localized methods on the L-shaped domain, a numerical solution to the eigenvalue problem from (1.1.2) can be found in the form of a set of numerical eigenfunctions and the corresponding eigenvalues. For the L-shaped domain, the collocation points were set

Table 3.1: First Ten Eigenvalues for L-shaped Domain Using 41×41 grid

Position	LMAPS	Kansa
1st	9.6204	9.7116
2nd	15.1009	15.2299
3rd	19.6198	19.7801
4th	29.6198	29.5236
5th	31.7534	31.9977
6th	41.1136	41.4228
7th	44.4399	44.7721
8th	48.8308	49.1933
9th	48.8308	49.1933
10th	56.2233	56.6370

up like a uniform grid which, on a square, would have been a 41×41 grid. However, since the domain is L-shaped, one quadrant of the square is omitted, leaving 1,281 collocation points of which 160 are boundary points and the rest are interior points. For ease in referencing, grids of different resolution on both the L-shaped and irregular domain will be referred to by the grid dimensions that would be applicable for a square domain. Thus, when talking about the grid with 1,281 collocation points, it will be denoted as the 41×41 grid. The shape parameter c in this study is chosen to be $c = \gamma d_s$, where d_s is the maximal distance from x_s to $\{x_k^{[s]}\}_1^n$; γ takes on values ranging from one to one hundred in increments of five.

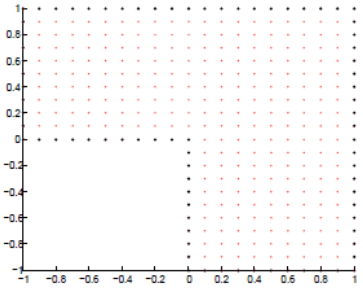

Figure 3.1: Collocation points for the 21×21 L-shaped grid

In calculating the numerical eigenfunctions and eigenvalues, the 5 nearest neighbors to each collocation point were used to compose the local domain for the approximation. The numerical eigenfunctions and eigenvalues were calculated using a $\gamma = 15$. Fifteen was chosen as the value for γ because, in the result of this study, it was shown to be a value that both minimizes the error and is relatively stable on the domain. Chapter 4 will provide a more in depth discussion of shape parameters and their influence on the numerical approximation as well as give justification for the previous statement.

In order to have a basis for comparison, the eigenvalues and numerical eigenfunctions were also found on the L-shaped domain by using localized Kansa's method. The parameters- value of γ, number of nodes, and number of contour lines- were kept consistent from the calculations using LMAPS. It is easy to notice that, between the two methods, the eigenvalues

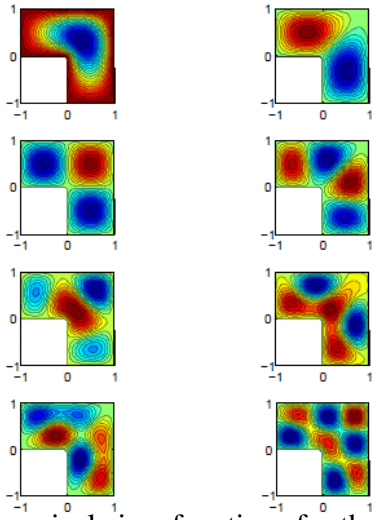

Figure 3.2: The first eight numerical eigenfunctions for the L-shaped domain using LMAPS.

are very similar. In most cases, the eigenvalues for localized Kansa's method are slightly larger than those calculated by LMAPS where the only exception is the fourth eigenvalue. Nevertheless, by inspecting the first ten eigenvalues, it appears as though both methods yield very similar numeric results.

In fact, the numerical eigenfunctions demonstrated the same degree of similarity. Since no visible differences could be detected, the numerical eigenfunctions calculated by using localized Kansa's method will not be displayed in this study. Figure 3.2 displays the first eight numerical eigenfunctions for the L-shaped domain which were generated by using LMAPS along with the same parameters as the eigenvalues in Table 3.1. Each numerical eigenfunction uses twenty contour lines.

3.2 Example 2: An Irregular Domain From The Northern Gulf of Mexico

A numerical approximation to the partial differential equation defined in (1.1.2) is calculated for the irregular domain in Figure 1.2 using both LMAPS and localized Kansa's method. The parameters for the meshless methods are set with slightly different values than those that were used for the L-shaped domain. The same shape parameter from the L-shaped domain results was used for the irregular domain. In addition, the collocation points were set up to

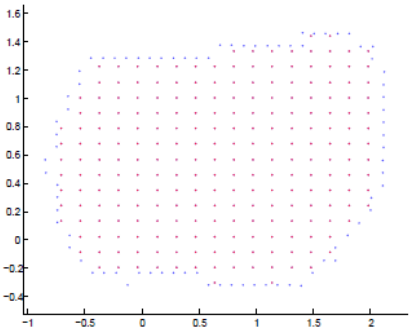

Figure 3.3: Collocation Points for Irregular Domain 21×21 Grid

be a uniform grid of the size 41×41 on a square domain. However, given that the domain is slightly irregular and more of a circular shape, the number of collocation points actually used to cover the domain was $1,018$ points with 80 boundary points. These boundary points were not generated by the uniform grid that populates the rest of domain. The boundary points were found by taking the latitude-longitude positions of surface current data for a given time slot and doing a simple transformation from the latitude-longitude coordinate system to an *x*-*y* coordinate system. From the set of *x*-*y* coordinates, the boundary points were manually identified to define the outline of the domain. The 21×21 and 41×41 grids for the irregular domain are the only time during which the boundary points are solely those that correspond to the surface current data collection sites. For uniform grid sizes with a higher resolution, i.e., 81×81, 161×161 and 321×321, extra boundary points were added to try to keep the grid size consistent throughout. For the 81×81 domain, all of the same boundary points were kept from the 41×41 grid and the midpoints between these points were added as boundary points. Similarly, the 161×161 grid and the 321×321 grid both kept all of the original boundary points and added points that would divide the distance between two consecutive boundary points in thirds and fourths, respectively.

Regardless of the grid size, within the domain, as previously stated, the collocation points are distributed on a uniform grid. However, some collocation points that would

Table 3.2: First Ten Eigenvalues for Irregular Domain using 41×41

Position	LMAPS	Kansa
1st	5.1333	5.1603
2nd	9.1630	9.1395
3rd	15.0432	15.0933
4th	16.6340	16.7839
5th	21.5634	21.4562
6th	23.8895	23.9831
7th	28.1992	28.2261
8th	33.8383	34.2456
9th	34.3436	34.4035
10th	37.6378	38.1084

have been a part of the uniform grid were omitted from the irregular domain if they were determined to be too close to the boundary. The criteria for being a point being omitted from the domain is if the distance from that point to any given boundary point is less than one-fourth of the smallest grid size in either the x or y direction.

Using these methods for populating the irregular domain with collocation points, both LMAPS and localized Kansa's methods were applied to the domain to calculate the eigenvalues and numerical eigenfunctions for the numerical approximation. For both methods, $\gamma = 15$ was used as the value for the shape parameter, and the local domains were based on the eight nearest neighbors. Justification for the choice of both of these values can be found in Sections 1 and 2 of the next chapter. Table 3.2 displays the eigenvalues for the first ten numerical eigenfunctions calculated by each method. As was found for the L-shaped domain, the eigenvalues calculated by localized Kansa's method are almost always slightly greater than the eigenvalues found through LMAPS, except for the second and fifth eigenvalues.

Figure 3.4 displays the first eight numerical eigenfunctions calculated for the irregular domain by using LMAPS. Each numerical eigenfunction uses twenty contour lines. Owing to the fact that no significant differences could be distinguished, the numerical eigenfunction for localized Kansa's method will not be displayed in this study.

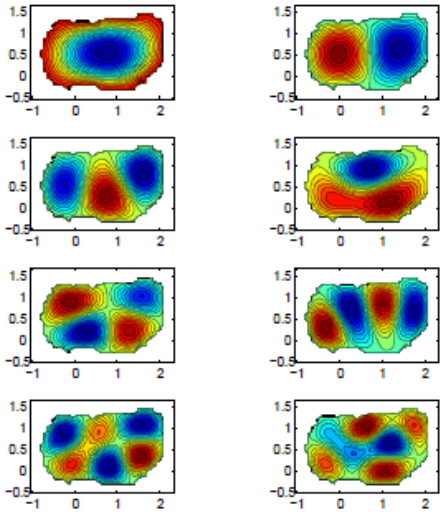

Figure 3.4: The first eight numerical eigenfunctions for the irregular domain using LMAPS.

Chapter 4

Conclusions and Remarks

LMAPS and localized Kansa's method were implemented to find the solution to the eigenvalue problem. Given the numeric approximation, a comparison of the accuracy and efficiency of the methods will be performed based on two sets of collocation points one for each type of domains. In this chapter, the results are provided for two types of comparisons that are made for both domains using both methods with various grid sizes. The first type of comparison is the relative error within eigenvalues which this study defines to be

$$\text{Relative error} = |\tilde{\lambda}^{(i)} - \tilde{\lambda_M}^{(i)}|/\tilde{\lambda}^{(i)},$$

where $i = 1, 2, \cdots, 8$ indicates which eigenvalue is being compared and M symbolizes the corresponding eigenvalue of a numeric approximation which utilizes a higher resolution grid. In this study, the relative error for the first eight eigenvalues of a domain will be graphed as it changes with different shape parameter values. In addition, this study will evaluate the maximum relative error of eigenvalues which is defined as

$$\text{Maximum relative error} = \max_{i=1,\ldots,8} \left(|\tilde{\lambda}^{(i)} - \tilde{\lambda}_M^{(i)}|/\tilde{\lambda}^{(i)} \right),$$

As with the relative error, the maximum relative error with be graphed in relation to changing shape parameter values. Calculating both the relative error and maximum relative error provides a basis for comparing the two methods on the same domain.

4.1 Remarks On The Shape Parameters

One of the more challenging issues in using LMAPS and localized Kansa's Method is determining a good value to use as the shape parameter for a given domain. In this section, both LMAPS and localized Kansa's methods were used with a variety of values for shape parameter. For both methods, the shape parameter $c = \gamma d_s$, where d_s is the maximal distance from x_s to $\{x_k^{[s]}\}_1^n$. In this way, d_s depends on the local domain of each collocation point. γ takes on values ranging from one to one hundred in increments of five. Although the γ value is what we are actually changing and testing in this section, we will refer to it as the shape parameter because the overall shape parameter, as previously defined, will increase with increased values in γ. In addition, the γ will be directly assigned values while the d_s value may vary over local domains. Nevertheless, the γ value will vary from one to one hundred in increments of five for the relative error and maximum relative error comparisons. Over this variation of shape parameter, the first comparison that is being made is relative error for eigenvalues of the first eight numerical eigenfunctions. Out of these calculations for relative error, the maximum relative error among the eight eigenvalues was determined for each shape parameter, and these are the values graphed in the second plot of each figure. Notice that analytic solution of this problem is not available. For both domains, the values of a lower resolution grid are compared with the next higher resolution grid. In this way, the 21×21 grid versus the 41×41 grid, the 41×41 grid versus the 81×81 grid are plotted in Figure 4.1, the 81×81 grid versus the 161×161 grid, the 161×161 grid versus the 321×321 grid are plotted in Figure 4.2. In this manner, the relative error and the maximum relative error were calculated and graphed for both domains using both methods and are displayed in Figures 4.1-4.10.

For the L-shaped domain, a local domain of five is used which would include the point itself and the four closest neighboring points. For an interior point, the value of d_s that factors into the shape parameter would be the same across the domain due to the uniform

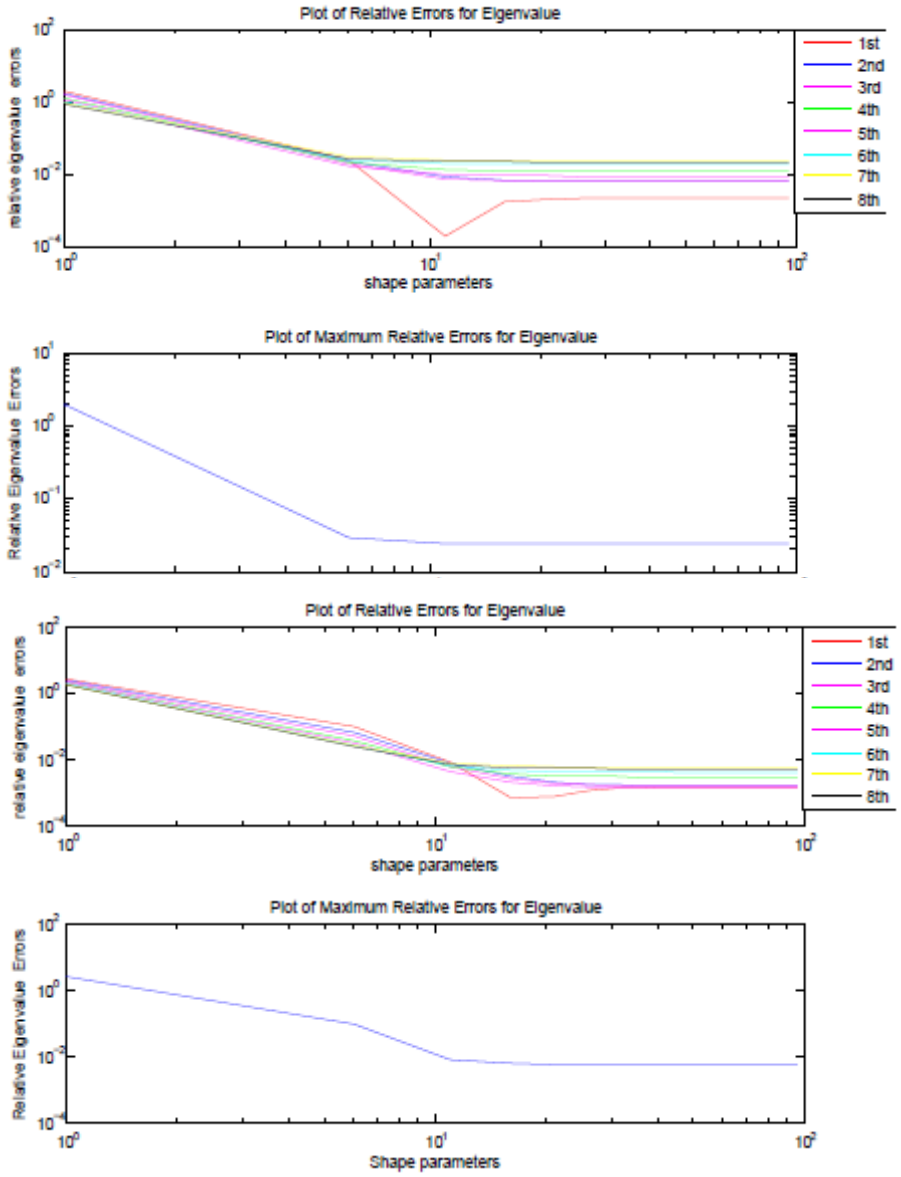

Figure 4.1: Localized Kansa's Method on L-shape domain, 21×21 versus 41×41; 41×41 versus 81×81.

grid of collocation points. For a boundary point, one or more of the points in the local domain would not be directly immediate neighbors. Thus, the value of d_s would take on a slightly larger value than for the boundary modes.

Using a local domain of five and various values for the shape parameter, Figure 4.1-4.2 displays the results of the relative error for the first eight eigenvalues and the maximum relative error over a range of shape parameters when localized Kansa's method is used for the L-shaped domain. Both comparisons for all four different grid comparisons yield smooths graphs demonstrating that that the error in the eigenvalues decrease with larger shape parameters, but, once the shape parameter hits a certain benchmark, the error levels off and remains consistent regardless of further increases in value. However, the benchmark value, after which the shape parameter is stable and the error becomes relatively constant, changes depending on the number of collocation points within the domain. As shown in Figure 4.1, for the 21×21 grid, the maximum relative error becomes stable near a shape parameter of five. However for the 321×321 grid, the maximum relative error does not stabilize until shape parameter reaches fifty. Nevertheless, all comparisons for localized Kansa's method demonstrate a certain level of smoothness

Unfortunately, Figure 4.3-4.4 demonstrates that LMAPS does not have the same degree of smoothness as characterized the results of localized Kansa's method. In fact, the comparisons of LMAPS on the L-shaped domain demonstrate the difficulty in trying to pick a shape parameter that will yield the highest possible degree of accuracy. For all four grid sizes, the error appears to drop for certain values of shape parameter followed by an increase in error of approximately 10^1 with only a small increase in shape parameter before the error falls back down again. The 21×21 grid is the only numerical approximation for which the comparisons produced a smooth graph comparable to localized Kansa's method. The other three grid sizes show greater variation in magnitude of error with respect to shape parameter. The comparisons for both methods were consulted when deciding a shape parameter value to use for looking at the convergence rates of both methods in the following section. As

shown in Figures 4.1-4.4, one hundred seems to be a good value for both methods and will be used in Section 4.3.

For the irregular domain, both localized Kansa's method and LMAPS were employed to run the same types of comparisons. However, in calculating the eigenvalues for which the relative error and maximum relative error were calculated, the local domain of the collocation points used eight nearest neighbors instead of five or nine. While eight may seem like a strange value because it does not produce a symmetric local domain, it was determined that, for this particular grid pattern, eight was the best size. To prove that eight was a better size for a local domain than the two symmetric domain sizes around it, the maximum relative error was calculated out of the first eight eigenvalues for a variety of shape parameter values using a local domain of five and nine. Both localized Kansa's method and LMAPS were tested using the 41×41 grid against the 81×81 grid.

In Figure 4.5, the maximum relative error decrease to between 1 and 0.1 at a shape parameter of 5 before the error starts increasing. Once it starts increasing, the error never gets to the low value it hit at 5. While the error varies less drastically using LMAPS, both localized Kansa's method and LMAPS show that the value of the shape parameter does not stabilize at a certain degree of error for any given range of shape parameters which makes it more difficult to chose a good shape parameter for this local domain arrangement. Therefore, using five nearest neighbors to make the local domain is not the most appropriate solution for the irregular domain.

To expand the local domain and keep it symmetric, nine was the next value that was tested for the local domain of each collocation point. The expectation was that nine points would provide a higher degree of accuracy than a local domain of five could yield. In addition, the goal was to find a local domain where the error would remain relatively constant after the shape parameter reached a benchmark value as had occurred with the L-shaped domain. However, as shown in Figure 4.6, the results did not agree with the expectation. For both methods, the error does eventually reach a low around 10 and 15 for

LMAPS and localized Kansa's Method, respectively. Unfortunately, the maximum relative error does not stabilize after this point. In contrast, shortly thereafter, the relative error begins a series of spikes where the variation in error between the high and low points is rather significant in magnitude, especially for localized Kansa's method. In this manner, the idea of using a local domain of nine points was discarded. In trying to find a good size for the local domain, values of six, seven, and eight were all tested with eight demonstrating the best results.

Thus, Figures 4.7-4.10 demonstrate the relative error and the maximum relative error for the first eight numerical eigenfunctions for shape parameters of different values using a local domain of eight. As was the case with the L-shape domain, a lower resolution is compared with the next highest resolution grid to calculate the values. Therefore, the 21×21 grid is compared to the 41×41 grid, the 41×41 grid compared to the 81×81 grid, the 81×81 grid compared to the 161×161 grid, and the 161×161 grid compared to the 321×321 grid.

For localized Kansa's method, the improvement upon local domains of size five or nine is quite significant, especially for the 41×41 grid. For this particular grid, the maximum relative error reaches its low around a shape parameter of ten and remains nearly constant afterwards. However, for the 81×81 and the 161×161 grids, the maximum relative error seems to stabilize after a benchmark shape parameter value, but, when the shape parameter takes a value from 55 to 100, the maximum relative error begins to oscillate rapidly. One possible explanation for these oscillations is due to the ill-conditioning of matrices for the local domain. With the increased number of points included in the local domain and the relatively large shape parameter, the matrices become near singular as the radial basis function values become dominated by the shape parameter value. Although these oscillations are not ideal, the shape parameter can accept a decent range, from 20 to 55, of values while maintaining a stable maximum relative error.

Figures 4.9-4.10 demonstrates an increased difficulty in picking an appropriate value

for a shape parameter. In particular, the 41×41 grid has a surprisingly large spike in error values from shape parameter 20 to 30 even though from 10 to 20 and 30 to 70 the maximum relative error is nearly constant. A spike appears for the same shape parameter values in the 81×81 grid comparison although it has a smaller magnitude and less stability in error for shape parameter values (6 to 21) leading up to the spike. The 161×161 grid also has some amount of fluctuation in the maximum relative error from shape parameter values 10 to 60 before the error stabilizes.

If the stabilized maximum relative error is compared between methods for the same grid size, then it appears as though both methods, for a stable shape parameter, provide the close to the same degree of accuracy. The key is to identify a good shape parameter for the method. Throughout this section, good ranges or values for the shape parameter have been identified for each method for each domain. By using the identified shape parameters on the appropriate domain with the correct method, the resulting numerical approximation can minimize its errors, and produce higher accuracy results.

4.2 Remarks On The Convergence Rates

In finding the convergence rate of both LMAPS and localized Kansa's method, the shape parameter was held constant at fifty for the L-shaped domain, and the irregular domain used a shape parameter of a hundred. The values for the shape parameters were chosen, based on the results from the previous section, to be fairly stable shape parameters for both methods. The L-shaped domain employed a local domain of the five nearest neighbors whereas the irregular domain broadened its local domain to include the eight nearest neighbors.

Table 4.1: Maximum Relative Error for L-Shaped Domain

Grid Size	LMAPS	Rate	Kansa	Rate
21*21	0.0317	—	0.0319	—
41*41	0.0076	2.0604	0.0077	2.0506
81*81	0.0017	2.1605	0.0018	2.0969
161*161	0.00049634	1.7761	0.00036831	2.2890

For the L-shape domain, the 321×321 grid size which translated to $77,441$ points and $1,280$ boundary points was taken to be the most accurate numerical approximation, and is, therefore, used as the basis for comparison. The first ten eigenvalues generated by the 320×320 grid size were compared in a pairwise fashion with the first ten eigenvalues for each of the 21×21, 41×41, 81×81, and 161×161 grid sizes. A maximum relative error was calculated for each of the four other grid sizes when compared with the 321×321 grid. The maximum relative error values are graphed corresponding to the grid size where the grid size is in terms of 21, 41, 81, 161 instead of the actual number of points in the grid which would be 341, $1,281$, $4,961$, and $19,521$, respectively. Table 4.1 gives the exact numerical results.

Clearly, LMAPS and localized Kansa's method converge at almost exactly the same rate for the L-shaped domain. The lines in the graph nearly coincide because the values are so close to each other with the exception being that LMAPS has a slightly larger maximum relative error for the 161×161 grid size. This data supports the observation in the previous section that the magnitudes of maximum relative error were comparable across methods for the L-shaped domain.

The same type of analysis was run on the irregular domain with a shape parameter of one hundred and local domain incorporating the eight closest neighbors to the given collocation point. The 321×321 will still be used for the basis of comparison, and it will be compared with the 21×21, 41×41, 81×81, and 161×161 grid sizes. These grid sizes correspond to 312 collocation points, $1,018$ collocation points, $3,924$ collocation points, and $15,270$ collocation points respectively. Nevertheless, the graph refers to the grid size as opposed to the number of collocation points. Table 4.2 displays the numerical results of the comparison.

While the values for the maximum relative error are close, they are not quite as close as the values for the L-shaped domain. A small amount of separation exists between the LMAPS values and the localized Kansa's method values. For the 41×41 grid, the LMAPS had a value approximately 1.75 times the localized Kansa's method value. However, for the

Table 4.2: Maximum Relative Error for Irregular Domain

Grid Size	LMAPS	Rate	Kansa	Rate
21*21	0.3543	—	0.0626	—
41*41	0.0223	3.9899	0.0132	2.2456
81*81	0.0030	2.8940	0.0037	1.8349
161*161	9.2815e-4	1.6925	0.0012	1.6245

higher resolution grids, the LMAPS values were slightly lower than the values for localized Kansa's method.

4.3 Conclusions

Overall, the maximum relative error for the two methods-LMAPS and localized Kansa's method- appear to converge at about the same rate regardless of whether the domain is a polygon, like the L-shaped domain, or slightly irregular, like the domain from the surface current data. The real difference between the methods seems to be in the stability of the shape parameter. Undoubtedly, there is a larger interval for the shape parameter for which localized Kansa's method is stable, as shown in Section 4.1, than the interval for which LMAPS is stable. The increased stability in localized Kansa's method is apparent for both domains. Thus, the results of this study demonstrate that using localized Kansa's method to find a numerical approximation to the eigenvalue partial differential equation in (1.1.2) would yield approximately the same magnitude of accuracy in the results as using LMAPS on the two given domains. In addition, finding a good shape parameter to use in the numerical approximation is easier with localized Kansa's method because there are less fluctuations in error as the shape parameter changes. Nevertheless, both methods have the capacity to produce results with a good degree of accuracy.

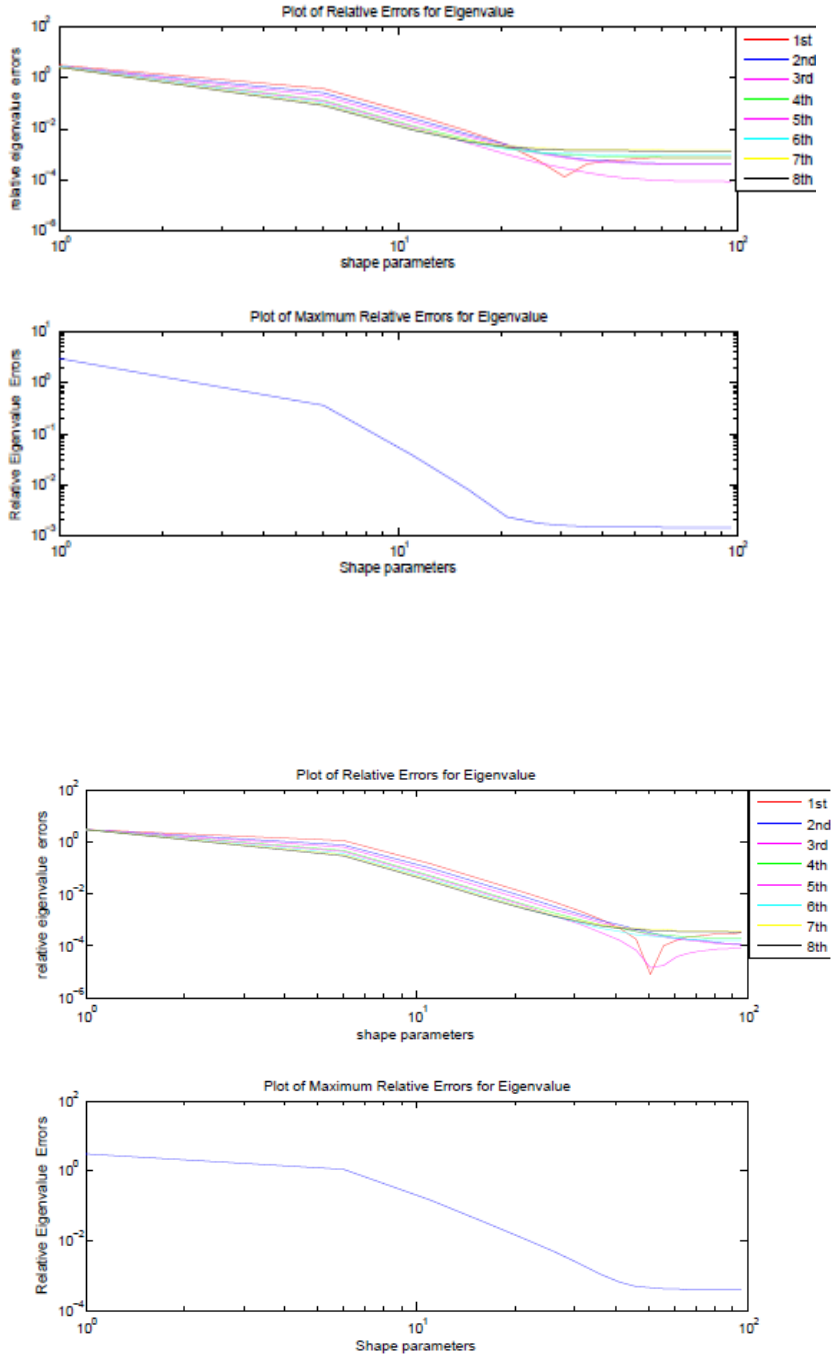

Figure 4.2: Localized Kansa's Method on L-shape domain, 81×81 versus 161×161; 161×161 versus 321×321.

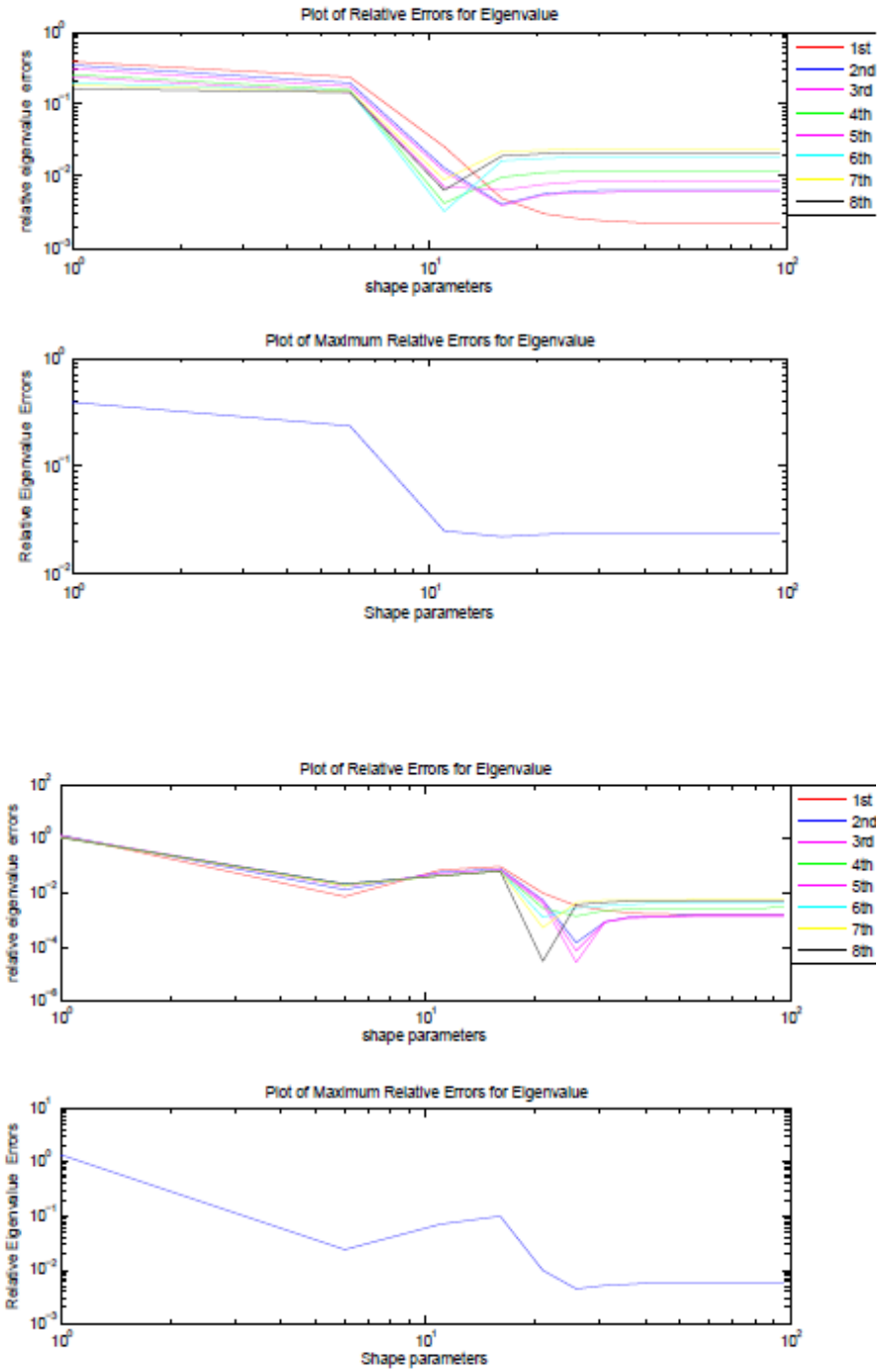

Figure 4.3: LMAPS on L-shape domain, 21×21 versus 41×41; 41×41 versus 81×81.

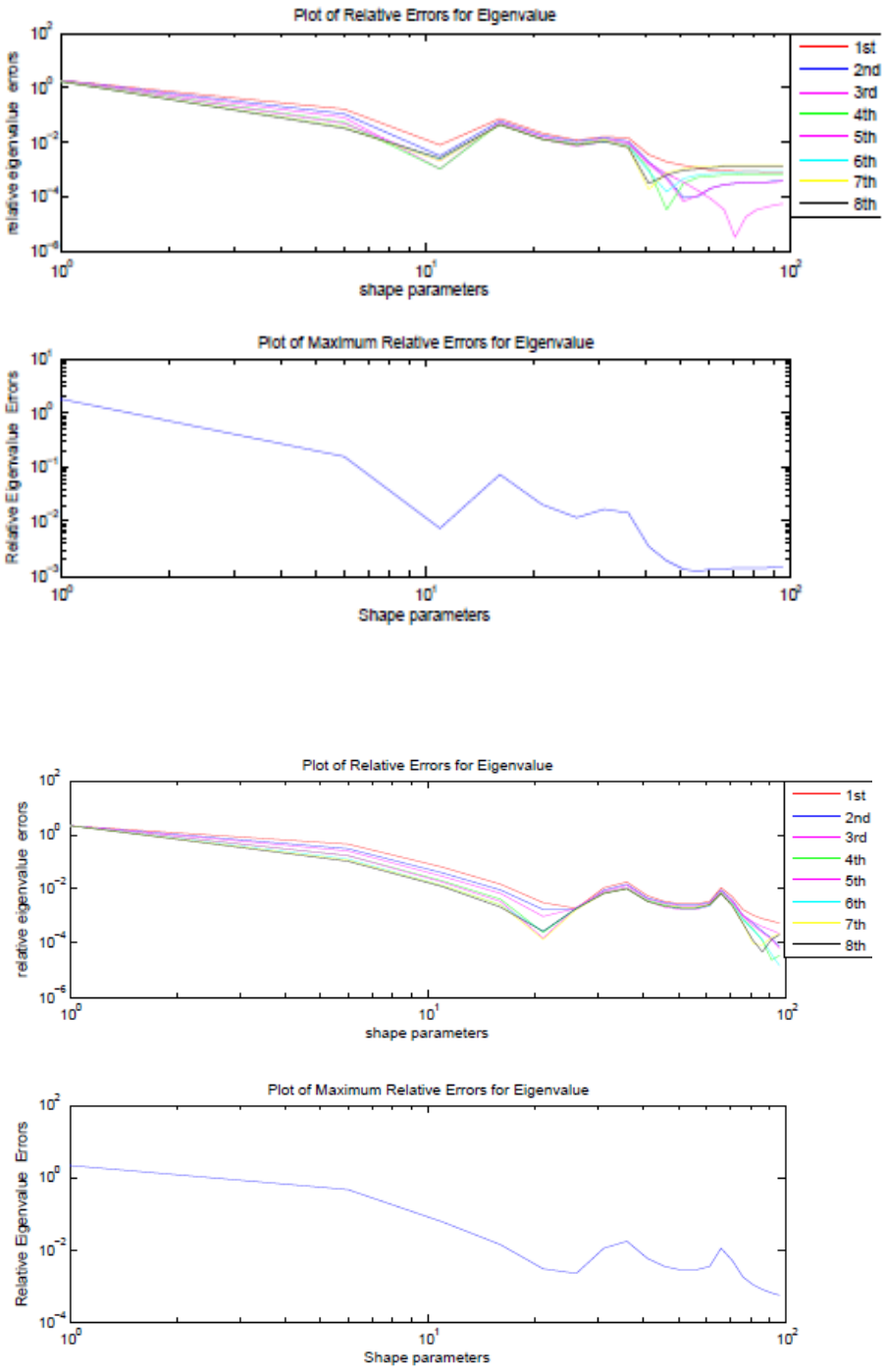

Figure 4.4: LMAPS on L-shape domain, 81×81 versus 161×161; 161×161 versus 321×321.

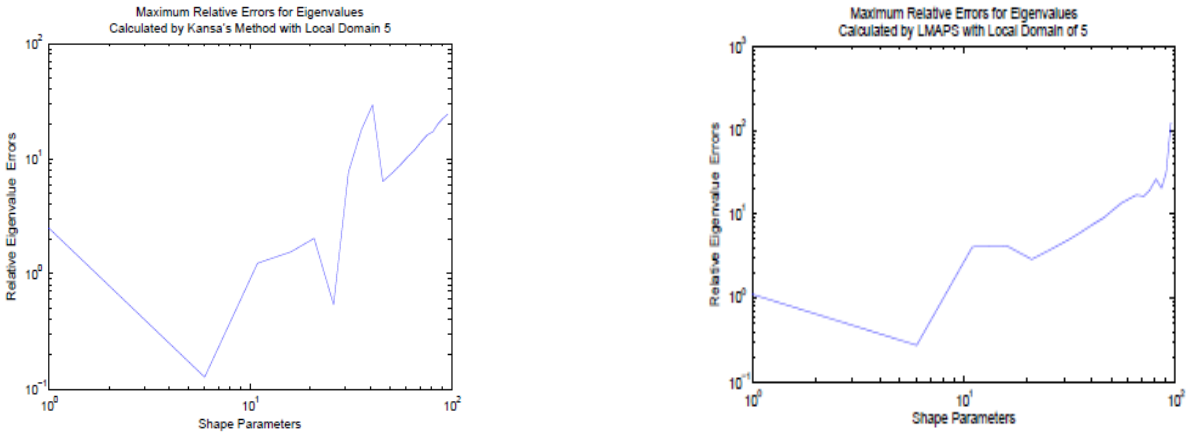

Figure 4.5: Errors of numerical eigenvalues using 5 local points.

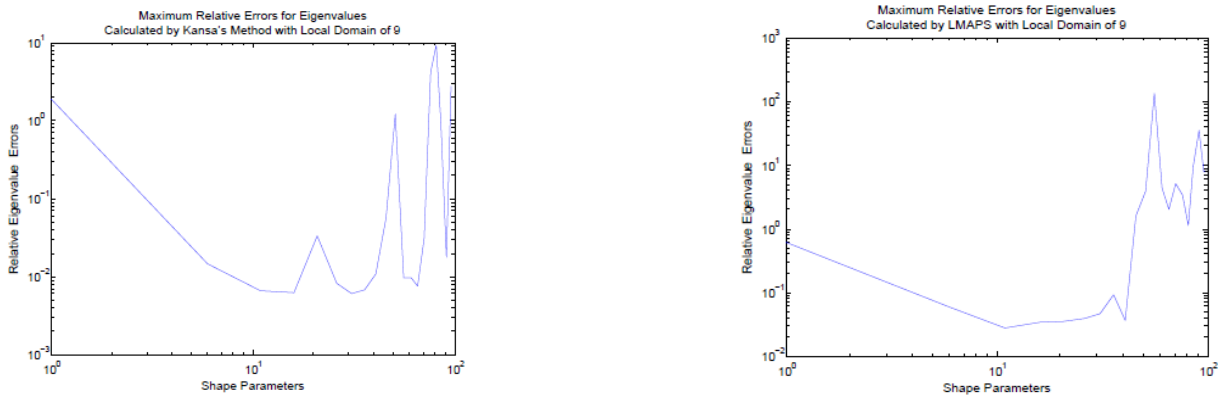

Figure 4.6: Errors of numerical eigenvalues using 9 local points.

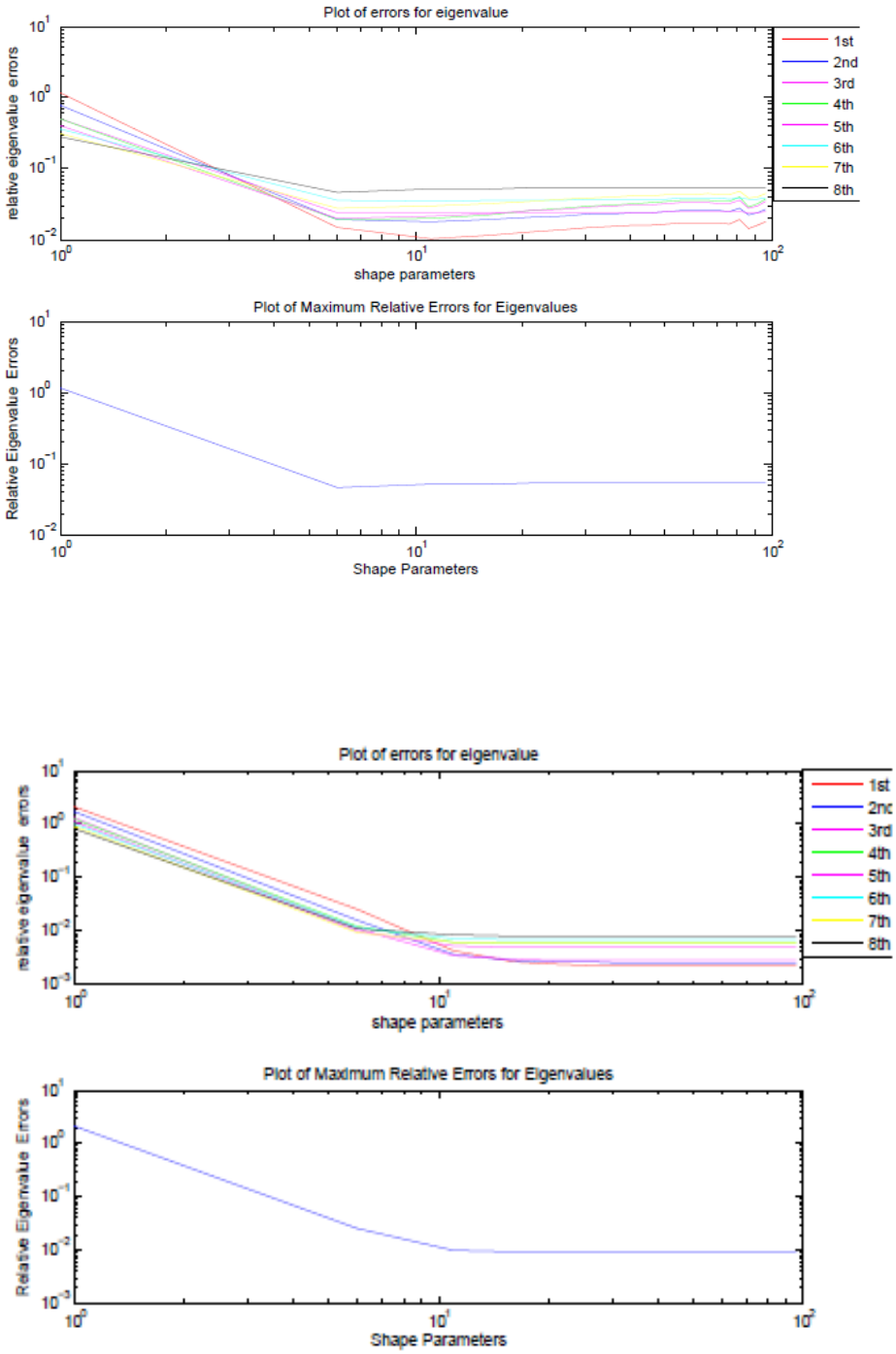

Figure 4.7: Localized Kansa's Method on irregular domain, 21×21 versus 41×41; 41×41 versus 81×81.

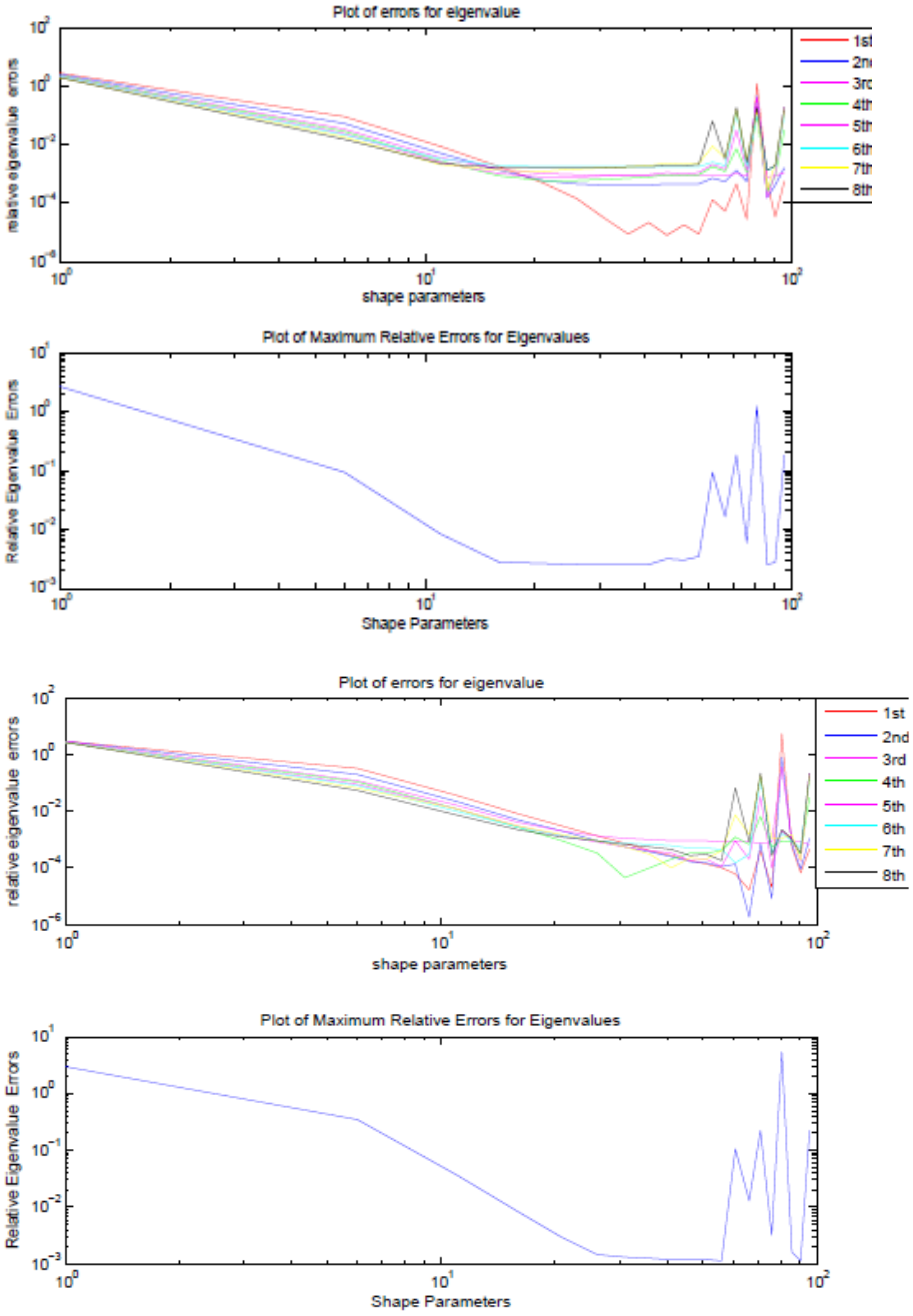

Figure 4.8: Localized Kansa's Method on irregular domain, 81×81 versus 161×161; 161×161 versus 321×321.

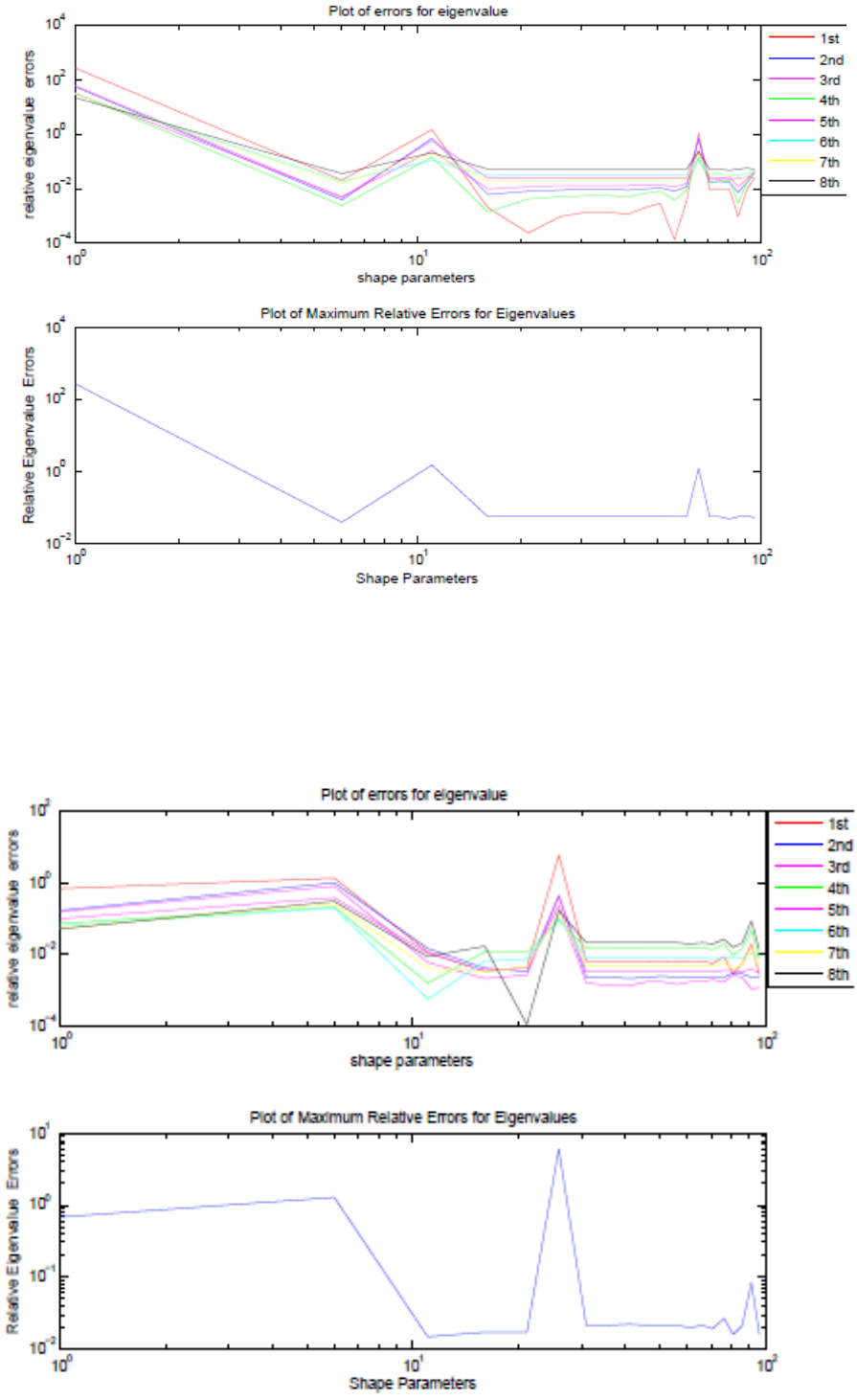

Figure 4.9: LMAPS on irregular domain, 21×21 versus 41×41; 41×41 versus 81×81.

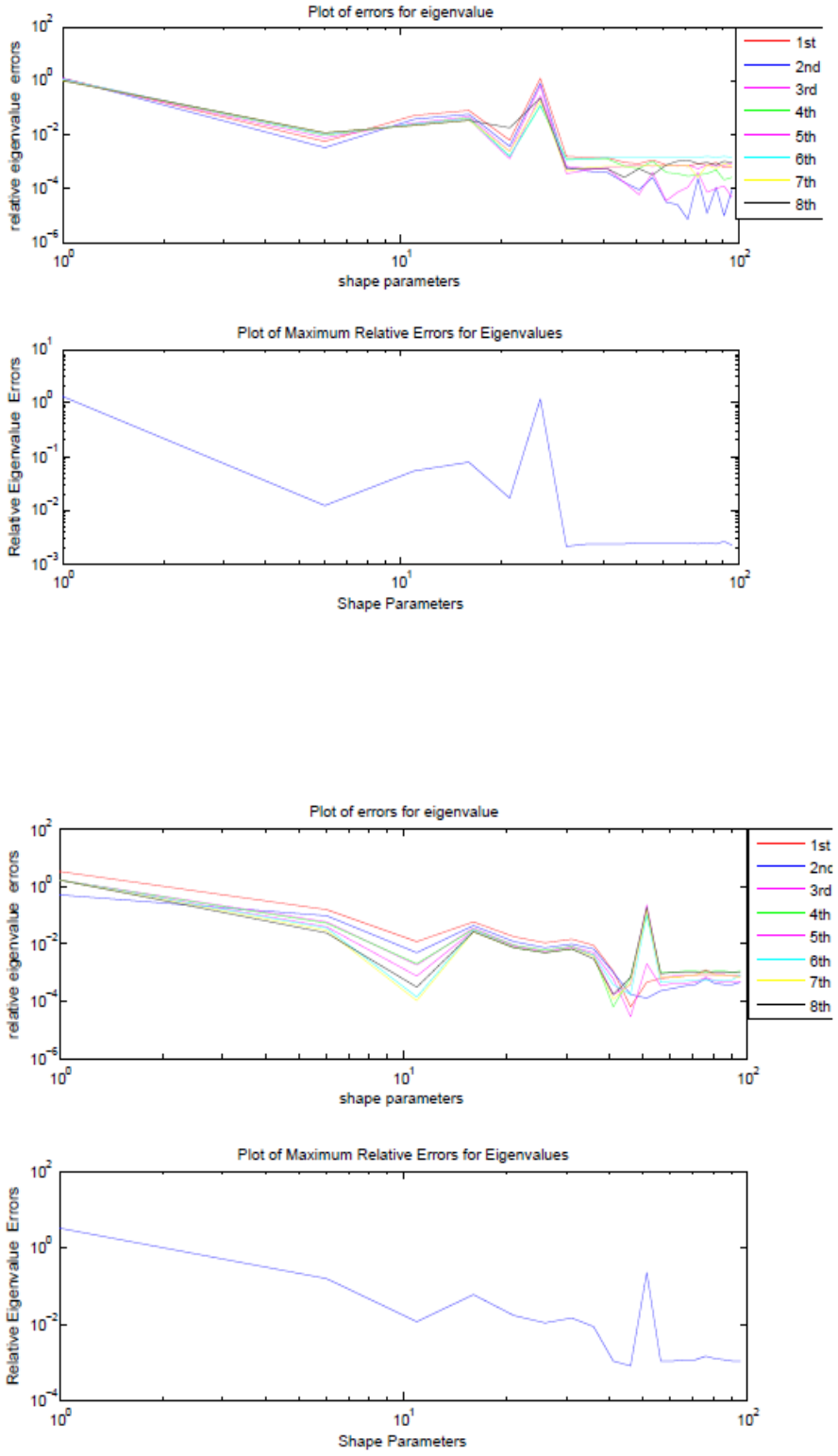

Figure 4.10: LMAPS on irregular domain, 81×81 versus 161×161; 161×161 versus 321×321.

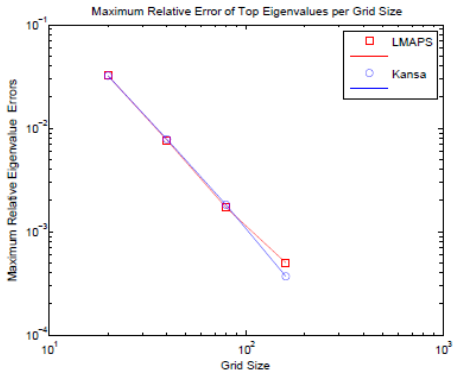

Figure 4.11: Convergence curves for L-shape domain.

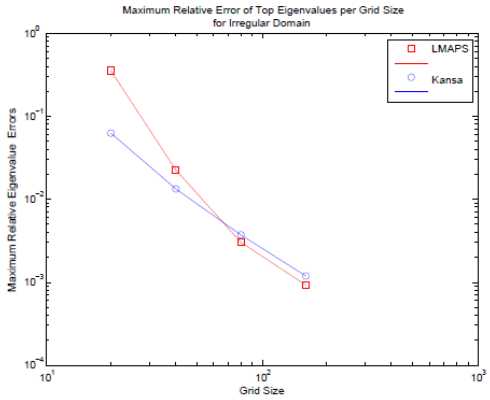

Figure 4.12: Convergence curves for irregular domain.

BIBLIOGRAPHY

[1] Anton, Howard and Chris Rorres. *Elementary Linear Algebra*. 9th ed. United States of America: John Wiley and Sons, Inc., 1973.

[2] Arfken, George B., Hans Weber, and Frank E. Harris. *Mathematical Methods for Physicists: A Comprehensive Guide.* 7th ed. Oxford: Elsevier Inc, 2013.

[3] Boffi, Danielle. *Finite Element Approximation of Eigenvalue Problems.* Cambridge University Press, 2010.

[4] Broomhead, D. S., and David Lowe. *Radial basis functions, multi-variable functional interpolation and adaptive networks*. (Technical Report 4148). RSRE. 1988.

[5] Chen, C.S., C.M. Fan and P.H. Wen, *The Method of Particular Solutions for Solving Certain Partial Differential Equations*, Numerical Methods for Partial Differential Equations, 28, 506-522, 2012.

[6] Chen, C.S., Y.C. Hon, and R.A. Schaback, *Scientific Computing with Radial Basis Functions*, 2012.

[7] Chu, Peter C, Leonid M. Ivanov, Tatiana P. Korzhova, Tatiana M. Margolina, and Oleg V. Melnichenko. *Analysis of Sparse and Noisy Ocean Current Data Using Flow Decomposition. Part I: Theory.* Journal of Atmospheric and Oceanic Technology 20.4 (2003): 478-491.

[8] Evans, Lawrence C. *Partial Differential Equations*. Vol. 19. Providence, Rhode Island: American Mathematical Society, 1998.

[9] Farlow, Stanley J. *Partial Differential Equations for Scientists and Engineers*. New York: Dover Publications, Inc., 1982.

[10] Hart, E.E., S.J. Cox, K. Djidjeli, and V.O. Kubytskyi, *Solving an eigenvalue problem with a periodic domain using radial basis functions*, Engineering Analysis with Boundary Elements, 33:258 - 262, 2009.

[11] Howden, Stephan D., Don Barrick and Hector Aguilar. *Applications of High Frequency Radar for Emergency Response in the Coastal Ocean: Utilization of the Central Gulf of Mexico Ocean Observing System during the Deepwater Horizon Oil Spill and Vessel Tracking.* Eds. Weilin W. Hou and Robert Arnone. *Proceedings of SPIE*. 2011, Bellingham,WA. 2011. Vol. 8030.

[12] Kansa, EJ. *Multiquadratic - a scattered data approximation scheme with applications to computational fluid dynamics - I. Surface approximations and partial derivatives estimates.* Comput Math Appl 19(8 - 9): 127 - 45, 1990.

[13] Kansa, EJ. *Multiquadratic - a scattered data approximation scheme with applications to computational fluid dynamics - I. Solution to parabolic, hyperbolic and elliptical partial differential equations.* Comput Math Appl 19(8 - 9):147 - 61, 1990.

[14] Khalaj-Amirhosseini, M., *Analysis of longitudinally inhomoge- neous waveguides using the method of moments*, Progress In Electromagnetics Research, Vol. 74, 57-67, 2007.

[15] Lekien, F., C. Coulliette, R. Bank, and J. Marsden. *Open-boundary modal analysis: Interpolation, extrapolation, and filtering. Journal of Geophysical Research* 109. C12004 (2004): 1-13.

[16] Lavranos, C.S.and G. A. Kyriacou, *Eigenvalue analysis of curved open waveguides using a finite difference frequency domain method employing orthogonal curvilinear coordinates*, PIERS Online, Vol. 1, No. 3, 271-275, 2005.

[17] Lipphardt, B. L., Jr., A. D. Kirwan Jr., C. E. Grosch, J. K. Lewis, and J. D. Paduan. *Blending HF radar and model velocities in Monterey Bay through normal mode analysis.* Journal of Geophysical Research 105.C2 (2000): 3425 - 3450.

[18] Lucy, L.B. *A Numerical approach to the testing of the fission hypothesis.* The Astronomical Journal 82.12 (1977): 1013-1024.

[19] Micchelli,Charles A. *Interpolation of Scattered Data: Distance Matrices and Conditionally Positive Definite Functions.* Constructive Approximation, 2 (1986): 11-22.

[20] Monaghan, J.J. *Why particle methods work.* SIAM Journal of Scientific and Statistical Computing 3.4 (1982):422-433.

[21] Platte, Rodrigo B. *Accuracy and Stability of Global Radial Basis Function Methods for the Numerical Solution of Partial Differential Equations*. Diss. University of Delaware, 2005.

[22] Platte, Rodrigo B. and Tobin A. Driscoll. *Computing Eignemodes of Elliptic Operators Using Radial Basis Functions*, Computers and Mathematics with Applications (2004).

[23] Powell,M.J.D. *Radial basis functions for multivariable interpolation: A review.* IMA conference on "Algorithms for the Approximation of Functions and Data." RMCS Shrivenham, (1985).

[24] Seydou, F., T. Seppanen, and O. M. Ramahi, *Computation ofthe Helmholtz eigenvalues in a class of chaotic cavities using the multipole expansion technique*, IEEE Transactions on Antennas and Propagation, Vol. 57, No. 4, 1169-1177, 2009.

[25] Arlett, P. L., A. K. Bahrani, and O. C. Zienkiewicz, *Application of finite element to the solution of Helmholtzs equation*, Proc. IEE.,15(12): 1762-1766, 1968.

[26] Trefethen, Lloyd N. and David Bau, III, *Numerical linear algebra*, SIAM 1997.

[27] Yao, Guangming. *Local Radial Basis Function Methods for Solving Partial Differential Equations*. Diss. University of Southern Mississippi, 2010.

[28] Yao, Guangming, C.S. Chen, Joseph Kolibal, *A localized approach for the method of approximated particular solutions*, Computers and Mathematics with Applications, 61, 2376-2387, 2011.